Hydrodynamic predictions for 5.44 TeV Xe+Xe collisions

Giuliano Giacalone,[1] Jacquelyn Noronha-Hostler,[2] Matthew Luzum,[3] and Jean-Yves Ollitrault[1]
[1]*Institut de Physique Théorique, Université Paris Saclay, CNRS, CEA, F-91191 Gif-sur-Yvette, France*
[2]*Department of Physics and Astronomy, Rutgers University, Piscataway, New Jersey 08854, USA*
[3]*Instituto de Física, Universidade de São Paulo, C.P. 66318, 05315-970 São Paulo, Brazil*

(Received 11 December 2017; published 6 March 2018)

We argue that relativistic hydrodynamics is able to make robust predictions for soft particle production in Xe+Xe collisions at the CERN Large Hadron Collider (LHC). The change of system size from Pb+Pb to Xe+Xe provides a unique opportunity to test the scaling laws inherent to fluid dynamics. Using event-by-event hydrodynamic simulations, we make quantitative predictions for several observables: mean transverse momentum, anisotropic flow coefficients, and their fluctuations. Results are shown as a function of collision centrality.

DOI: 10.1103/PhysRevC.97.034904

I. INTRODUCTION

Relativistic hydrodynamics has proven successful in describing the evolution of the system formed in ultrarelativistic nucleus-nucleus collisions [1–5]. Typical signatures of hydrodynamics, such as elliptic flow [6] or jet quenching [7], depend on simple macroscopic properties of the quark-gluon medium, such as its shape and size. Challenging tests of this macroscopic description can therefore be performed by studying how observables evolve under variations of the medium geometry. To achieve this, one can either study a given colliding system in various centrality windows, or collide different species of nuclei with significant variation in the mass numbers.

So far, in addition to $p+p$ collisions, ^{208}Pb + ^{208}Pb [8] and $p+^{208}$Pb collisions have been carried out at the CERN Large Hadron Collider (LHC). While there seems to be a consensus that hydrodynamics applies to collisions between heavy nuclei, there is still a debate as to whether typical signatures of a quark-gluon plasma observed in small systems [9–11] (e.g., the ridge [12–14], or multiparticle correlations [15–17]) are also of hydrodynamic origin or not [18–22]. On October 9, 2017, an 8-h run of collisions between ^{129}Xe nuclei at a center-of-mass energy of 5.44 TeV was carried out at the LHC. The mass number of xenon being roughly halfway between that of a proton and that of a lead nucleus, upcoming data from the Xe+Xe run offer a unique possibility to test the predictive power of the hydrodynamic framework under simple, though substantial, variations of the geometry of the quark-gluon plasma.

The effects of varying the mass number A of the colliding nuclei can be evaluated using scaling laws, which play an important role in fluid dynamics. Both the number of observed particles [23–26] and the volume of the fluid are proportional to A, so that the density of particles per unit volume is essentially independent of A. Varying A amounts, in a first approximation, to scaling all space-time variables by $A^{1/3}$. Now, ideal hydrodynamics is scale invariant: The distribution of temperature and fluid velocity is strictly unchanged upon such a linear rescaling. This implies that, for instance, to a good approximation transverse momentum spectra up to $p_t \sim 2$ GeV should be identical in Xe+Xe and Pb+Pb collisions. Scale invariance, however, is a rough approximation, which is broken by several effects:

(i) The surface thickness of a nucleus, $a \sim 0.5$ fm, is independent of A, so that the boundary of smaller nuclei is relatively less sharp. This leads to a smaller eccentricity in the reaction plane for smaller systems [27], which in turn implies a smaller elliptic flow in mid-central collisions.

(ii) Short-range fluctuations [28] of the initial density profile. Their spatial extension is determined by the microscopic collision dynamics and is likely to depend little on A. Their effect is typically proportional to $A^{-1/2}$ [29]. They explain why elliptic flow is sizable even in central collisions, and why it is larger for smaller A [27]. These fluctuations are also responsible for triangular flow [30].

(iii) The viscous corrections to ideal hydrodynamics,[1] which involve gradients [33], and whose effects are, therefore, proportional to $A^{-1/3}$. Their main effect is to decrease the hydrodynamic response to the initial anisotropies [34].

(iv) The ^{208}Pb nucleus is spherical while ^{129}Xe has a moderate prolate deformation [35].

Precise comparisons between Pb+Pb and Xe+Xe data will provide an exceptional opportunity of verifying these scaling rules, which lie at the heart of the hydrodynamic modeling.

The main limitations of the hydrodynamic framework are the poor knowledge of the initial density profile, and of the unknown transport coefficients (viscosity) of the quark-gluon plasma [36,37]. Some models of the initial density can be ruled out by combining elliptic and triangular flow data [38], in the sense that they do not yield good descriptions of experimental

[1]By viscous corrections, we mean here *all* departures from local equilibrium: in the hydrodynamic modeling, they are due not only to the viscosity during the fluid phase, but also to the traditional freeze-out procedure [31], which effectively takes into account the departure from equilibrium at the end of the evolution [32].

data even after tuning the viscosity. Nevertheless, even if a particular model of initial conditions can be made compatible with data at the expense of adjusting the viscosity, it is not guaranteed that it provides an accurate representation of reality.[2]

We can argue, though, that if a particular hydrodynamic calculation matches Pb+Pb data, it should correctly predict Xe+Xe data, even if it has the wrong initial conditions and viscosity. The uncertainty in initial conditions comes from the microscopic dynamics, not from the structure of the nuclei: If a model of initial conditions overestimates both eccentricity and fluctuations in Pb+Pb collisions, it is likely to also overestimate them by the same fraction in Xe+Xe collisions. It should be stressed that the error on initial conditions will not be exactly compensated by the error on the viscosity, because viscous damping is larger in smaller systems. However, this is a small change, because viscous effects are proportional to $A^{-1/3}$, so that they increase only by 17% from ^{208}Pb to ^{129}Xe. Therefore, even though we do not have control over all the features of the hydrodynamic modeling, we are able to make robust predictions for the system size dependence of typical hydrodynamic signatures.

We focus on a few bulk, soft observables, which allow us to test directly the hydrodynamic scaling: mean transverse momentum, anisotropic flow, and flow fluctuations. We do not study in detail the dependence of yields or flow on transverse momentum, pseudorapidity, or particle type. Simulations are carried out for both Pb+Pb collisions at $\sqrt{s_{\rm NN}} = 5.02$ TeV, and Xe+Xe collisions at $\sqrt{s_{\rm NN}} = 5.44$ TeV. In Sec. II, we present the details of the initial condition model used in this paper, and the setup of our hydrodynamic code. Results are presented in Sec. III.

II. HYDRODYNAMIC MODELING

Since we do not study the rapidity dependence of observables, we assume that the longitudinal expansion of the medium is boost invariant [39]. In each event we specify the initial density profile over the transverse plane, and then determine the transverse expansion numerically using a 2+1 dimensional hydrodynamic code.

A. Initial state

The model of initial conditions that we shall use throughout this paper is the TRENTo model with $p = 0$ (we refer to [40] for a detailed description of this model). In this model, the total entropy deposited at a given point in the transverse plane after the collision is calculated as $\sqrt{T_A T_B}$, where T_A and T_B are the thickness functions of the incoming nuclei at that point.[3] In the remainder of this section we shall explain that this choice of initial state model is strongly motivated by experimental results on Pb+Pb collisions.

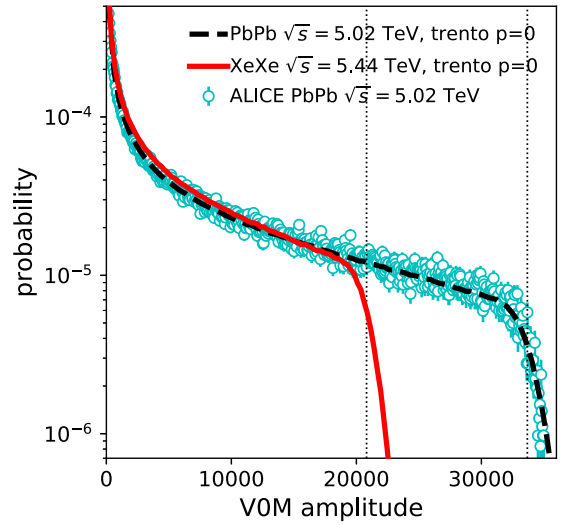

FIG. 1. Probability distribution of the V0M amplitude, used by the ALICE Collaboration to sort events into centrality classes [42]. Symbols: ALICE data for 5.02 TeV Pb+Pb collisions. Dashed line: Rescaled TRENTo entropy in 5.02 TeV Pb+Pb events. Full line: Prediction for 5.44 TeV Xe+Xe collisions using the same model. The vertical dotted lines indicate the locations of the knees of the histograms (see text for more details).

1. Multiplicity and centrality

In experiment, the centrality of a nucleus-nucleus collision is defined according to the transverse energy [43,44] or multiplicity [45] in a detector. While these are, strictly speaking, final-state observables, they mostly reflect the initial entropy of the medium for the following reasons: The entropy increase due to viscosity during the hydrodynamic phase is typically a small fraction, and the transverse energy per particle depends little on centrality. Therefore, one can assume that the quantity used to determine the centrality is proportional to the initial entropy. Within this assumption, the TRENTo model with $p = 0$ is very successful in reproducing distributions of multiplicity measured at the LHC in Pb+Pb collisions [40]. We show in Fig. 1 the distribution of entropy obtained in this model, which we shall later use to sort events into centrality classes. We compare it to the distribution of the V0M amplitude used by the ALICE Collaboration to perform the centrality determination in Pb+Pb collisions at $\sqrt{s_{\rm NN}} = 5.02$ TeV [42]. The values of entropy provided by TRENTo are rescaled on the horizontal axis, so that the histogram of the model and that of ALICE data present the same *knee*, which, following [46], is defined as the mean value of the V0M amplitude at zero impact

[2]A model may, for instance, underestimate both the initial eccentricity and the density fluctuations. A good description of data could be achieved, then, through an overestimation of the hydrodynamic response to the initial anisotropies, i.e., by implementing a smaller viscosity.

[3]The Woods-Saxon parametrization used for shaping the ^{129}Xe nuclei is taken from Ref. [41] for what concerns the surface thickness a and the nuclear radius R. The shape parameters characterizing the deformation of the nucleus are instead taken from Ref. [35]. Thus, our Xe nuclei present $A = 129$, $R = 5.42$ fm, $a = 0.57$ fm, $\beta_2 = 0.162$, $\beta_4 = -0.003$.

parameter.[4] Once the knees are matched, histograms are in perfect agreement. To be more quantitative, we check that the fraction of events on the right of the knee, i.e., the centrality of the knee, $c_{\rm knee}$, is correctly reproduced by the model.[5] Indeed, we obtain $c_{\rm knee} = 0.39 \pm 0.02\%$ in TRENTo, while ALICE data present $c_{\rm knee} = 0.38 \pm 0.04\%$. We stress that this quantity is independent of the calibration of the measured multiplicity (horizontal axis).

A second nontrivial success of this model is that it captures correctly the dependence of multiplicity on the system size. We can check this explicitly using the Relativistic Heavy-Ion Collider (RHIC) data on Cu+Cu and Au+Au collisions at $\sqrt{s_{\rm NN}} = 200$ GeV. The $p = 0$ model predicts the multiplicity of central Au+Au collisions to be 3.5 times larger than that of central Cu+Cu collisions. This is a bit larger than scaling expected from the ratio of the mass numbers, $197/63 \simeq 3.1$, and turns out to be in agreement with RHIC data, as the multiplicity of charged particles measured in Au+Au collisions is larger by a factor 3.8 [48].

Motivated by these features, we show in Fig. 1 the prediction of the $p = 0$ model for the histogram of the V0M amplitude in Xe+Xe collisions at $\sqrt{s_{\rm NN}} = 5.44$ TeV. We predict $c_{\rm knee} = 0.51 \pm 0.04\%$ in Xe+Xe collisions. Note that, the centrality of the knee being due to fluctuations, it follows to a good extent the expected $A^{-1/2}$ scaling, as $(129/208)^{-1/2} \approx 0.51/0.39$.

2. *Initial anisotropies*

The other crucial aspect of the initial state model is that it provides the medium with a geometry and its anisotropies, which are known to leave peculiar phenomenological signatures. In particular, the most prominent momentum anisotropies of the final-state particle distribution, elliptic flow, and triangular flow arise mainly from the eccentricity ε_2 and triangularity ε_3 of the system [49], respectively. The $p = 0$ model is known to yield anisotropies which are compatible with experimental data, in the sense that it presents rms ε_2 and ε_3 which pass the test proposed in Ref. [38] across the full centrality range. Further, relative fluctuations of ε_2 in this model turn out to be in good agreement with data on multiparticle cumulants of elliptic flow in central collisions [50]. In Fig. 2(a), we present the rms eccentricities and triangularities predicted by the TRENTo model as a function of centrality percentile, in both Pb+Pb and Xe+Xe collisions.

The triangular anisotropy of the medium, ε_3, is not expected to be dynamically generated by the fluctuations of orientations of the deformed ^{129}Xe nuclei, and it is solely due to density fluctuations in both Xe+Xe and Pb+Pb. Therefore, it is larger

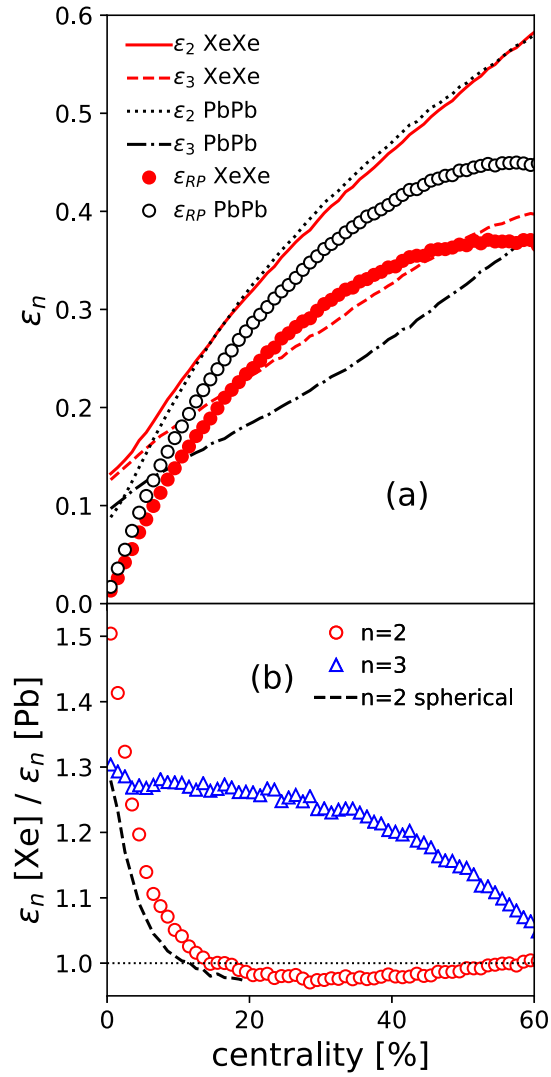

FIG. 2. (a) Root-mean-square values of the initial eccentricity ε_2 and the initial triangularity ε_3 [51] in the TRENTo model, as a function of centrality percentile, in Pb+Pb collisions at $\sqrt{s_{\rm NN}} = 5.02$ TeV, and Xe+Xe collisions at $\sqrt{s_{\rm NN}} = 5.44$ TeV. ε_{RP} denotes the mean value of the eccentricity in the reaction plane [27]. (b) Ratio of rms ε_2 and ε_3 between Xe+Xe and Pb+Pb collisions. The dashed line in this panel is the result for ε_2 obtained by switching off the deformation of the Xe nucleus (see text).

if the system is smaller, and it increases with the centrality percentile for a given system, and it is larger in Xe+Xe collisions than in Pb+Pb collisions at the same centrality percentile. Figure 2(b) shows that the ratio between the initial triangularities of Xe+Xe and Pb+Pb collisions is close to 1.27 for most centralities, in agreement with the expected $A^{-1/2}$ scaling.

The eccentricity ε_2 on the other hand, gets contribution from both fluctuations and the almond shape of the system due to a finite impact parameter, which is quantified by the mean eccentricity in the reaction plane, dubbed $\varepsilon_{\rm RP}$ in the figure. Fluctuations and $\varepsilon_{\rm RP}$ add in quadrature [52]: $\varepsilon_2 = \sqrt{\varepsilon_{\rm RP}^2 + \sigma^2}$, where σ^2 denotes the variance of ε_2 fluctuations. The reaction

[4] Alternatively, one can define the knee as the rightmost inflection point if one plots the probability of Fig. 1 in a linear scale, instead of a logarithmic scale [47]. Both methods are essentially equivalent.

[5] The TRENTo calculation shown in Fig. 1 implements a fluctuation parameter $k = 2.0$, which is found to provide the best agreement with the measured $c_{\rm knee}$. The TRENTo events that shall be used as initial condition for the hydrodynamic evolution, on the other hand, present $k = 1.6$, as suggested in [2]. This value gives a $c_{\rm knee}$ that is slightly too large, but the difference has a negligible effect on the observables presented in Sec. III.

plane eccentricity $\varepsilon_{\rm RP}$ is larger in Pb+Pb than in Xe+Xe at all centralities, which is explained by the sharper nuclear surface of the Pb+Pb system. In central collisions, however, $\varepsilon_{\rm RP}$ vanishes and ε_2 is solely due to fluctuations: It is of the same order as ε_3 in both systems. Hence, ε_2 is larger in Xe+Xe than Pb+Pb for central collisions, but smaller for mid-central collisions [Fig. 2(b)]. Note that in very central collisions the ratio of the ε_2 coefficients presents a significant deviation from the value 1.27 expected from $A^{-1/2}$ scaling. This is due to the prolate shape of the ^{129}Xe nuclei, in particular, to a nonzero value of the parameter β_2. The random orientation of the colliding nuclei provides a dynamical source of eccentricity fluctuations, which dominates over density fluctuations in central collisions, as is known, for instance, from experimental investigations of ^{238}U + ^{238}U collisions [53]. For completeness, then, the dashed line in Fig. 2(b) indicates the ratio of eccentricities that one would obtain if ^{129}Xe nuclei were spherical, i.e., by setting $\beta_2 = \beta_4 = 0$ in the Woods-Saxon parametrization. As expected, this ratio in central collisions naturally follows the $A^{-1/2}$ scaling. The effect of deformation is therefore maximum at 0% centrality, where it increases by 15% the value of ε_2, and disappears around 20% centrality.

B. Hydrodynamic evolution

We sort a sample of few million TRENTo simulations ($p = 0$, $k = 1.6$, $\sigma = 0.51$) of both Pb+Pb collisions at $\sqrt{s_{\rm NN}} = 5.02$ TeV and Xe+Xe collisions at $\sqrt{s_{\rm NN}} = 5.44$ TeV into centrality classes, through bins of 5% width, from 0% to 60% centrality. In each bin we evolve hydrodynamically approximately 2200 events, for both systems. Each initial density profile is evolved by means of the viscous relativistic hydrodynamical code V-USPHYDRO [54–56].

The equation of state (PDG16+/2+1[WB]) we use is that recently calculated on the lattice with three quark flavors (u, d, s) and physical quark masses [57]. We start the hydrodynamic evolution at a time $\tau_0 = 0.6$ fm/c after the time of collision [58]. We neglect the transverse expansion before τ_0 [59–62]. Doing so, we underestimate the transverse flow, which we partially compensate with the implementation of a low shear viscosity over entropy ratio, $\eta/s = 0.047$ [63]. The bulk viscosity [54,55,64–66] is set to zero in our calculation. These parameters are the same used in Ref. [63], and were chosen so as to reproduce experimental data on Pb+Pb collisions at $\sqrt{s_{\rm NN}} = 5.02$ TeV. We run hydrodynamics until the temperature drops below 150 MeV, at which point the fluid transforms into hadrons [67]. Therefore, we do not implement any hadronic afterburner prescription (such as UrQMD), which may further explain why best fits to data are achieved within our code using a lower value of η/s than in Ref. [2].

The equation of state of the fluid matches to a hadron resonance gas model with the most up-to-date particles from the Particle Data Group that includes all *-**** resonances [68], which are shown to be needed from first principles [69]. All these hadronic resonances can be formed during the freeze-out process. We neglect rescatterings in the hadronic phase [70], but implement strong decays of all hadronic resonances into stable hadrons using an adapted version of the decay code of [71].

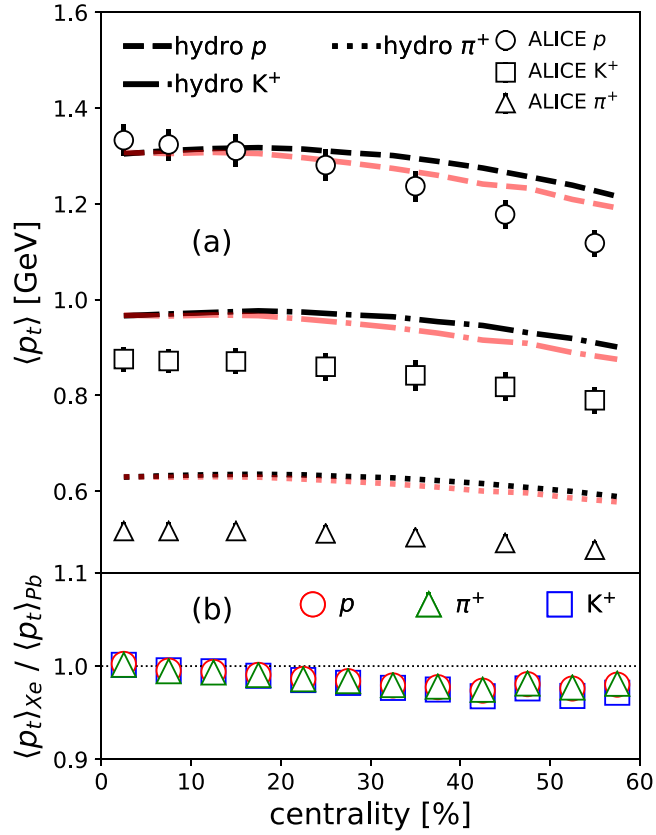

FIG. 3. (a) Mean transverse momentum $\langle p_T \rangle$ of identified particles as a function of centrality percentile. Symbols: ALICE results for Pb+Pb collisions at $\sqrt{s_{\rm NN}} = 2.76$ TeV [72]. Black lines: Our hydrodynamic results for Pb+Pb collisions at $\sqrt{s_{\rm NN}} = 5.02$ TeV. Grey lines: Our hydrodynamic results for Xe+Xe collisions at $\sqrt{s_{\rm NN}} = 5.44$ TeV. Panel (b) displays the ratio between Xe+Xe and Pb+Pb collisions.

III. RESULTS

A. Transverse momentum spectra

Figure 3(a) displays the mean transverse momentum of pions, kaons, and protons in our hydrodynamic calculation as a function of the centrality percentile. We present our results along with ALICE data at a lower energy [72], since identified particle spectra at $\sqrt{s_{\rm NN}} = 5.02$ TeV have not been published yet.

The mean transverse momentum is remarkably independent of centrality, both in hydrodynamics and in experiment. This flatness of data is a robust prediction of the hydrodynamic framework, and the fact that it is observed experimentally strongly supports the validity of the hydrodynamic approach. We find that the absolute value of $\langle p_{\rm T} \rangle$ is larger in our calculation than in data, for pions and kaons. The discrepancy is larger than that expected simply from the different colliding energy, which should yield a 3% variation [73]. Agreement could be improved by adding a bulk viscosity [74].

However, our goal in this paper is to predict how $\langle p_T \rangle$ *evolves* between Pb+Pb and Xe+Xe collisions. The ratios of mean transverse momenta for different particle types are

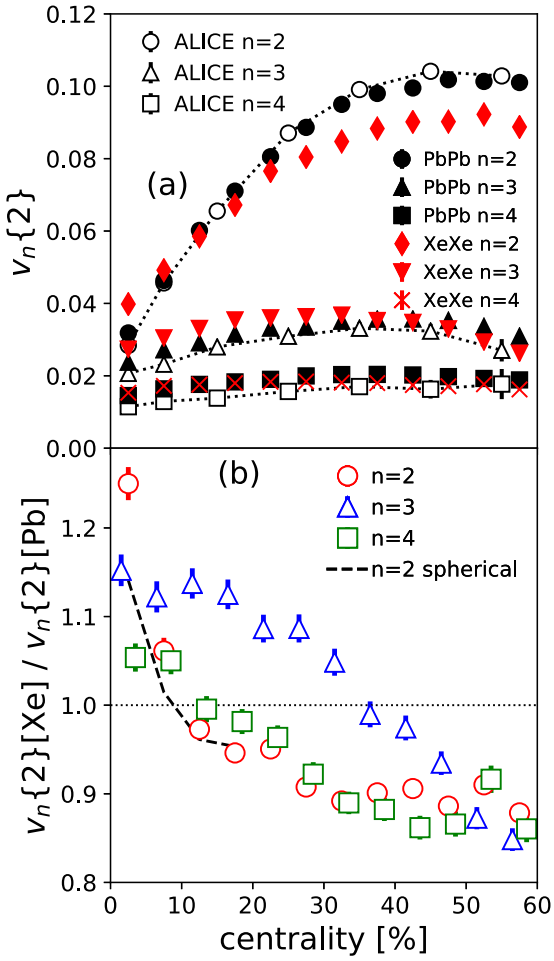

FIG. 4. (a) rms values of v_2, v_3, and v_4 as a function of collision centrality. Open symbols: ALICE data for Pb-Pb collisions at $\sqrt{s_{\rm NN}} = 5.02$ TeV [78]. Full symbols: our hydrodynamic calculations for Pb+Pb and Xe+Xe collisions. The kinematic cuts are $0.2 < p_T < 5$ GeV/c and $|\eta| < 0.8$. (b) Hydrodynamic predictions for the ratios of the rms anisotropies between Xe+Xe and Pb+Pb collisions. The dashed line in this panel is the result for v_2 obtained by switching off the deformation of the Xe nucleus.

plotted in Fig. 3(b). The ratios are very close to unity, as expected from the scale invariance of fluid dynamics, and the fact that the effective density [75] is essentially identical in both systems. Note that the increase of the energy per nucleon pair from 5.02 to 5.44 TeV between Pb+Pb and Xe+Xe collisions only has a small effect. It entails an increase of the multiplicity by 2.5% [76] which, in turn, implies an increase of the mean transverse momentum by 0.5% [73].

B. Anisotropies

The anisotropies of the azimuthal distribution of charged particles are quantified by the Fourier coefficients v_n [77], and represent a distinctive signature of collective behavior. Figure 4(a) displays the rms value of v_n, denoted by $v_n\{2\}$ [79], for $n = 2,3,4$, as a function of centrality percentile. Our calculation for Pb+Pb collisions is in good agreement with ALICE data. It slightly overestimates v_4 and, to a lesser extent, v_3, which could be improved by increasing the shear viscosity, as viscous damping becomes more important for higher harmonics [80,81]. Figure 4(b) displays our prediction for the ratios of $v_n\{2\}$ between Xe+Xe and Pb+Pb collisions. We expect these ratios to be independent of kinematic cuts in p_t and η, and thus our prediction to be independent of the experimental setup.

Now, v_2 and v_3 are to a good approximation proportional to ε_2 and ε_3 [82], i.e., $v_n = \kappa_n \varepsilon_n$. In ideal hydrodynamics, the response coefficient κ_n is independent of the system size and shape. Viscous corrections decrease κ_n by an amount proportional to $1/R$, where R is the transverse size [83]. Hence, for a given system κ_n decreases as a function of centrality percentile, whereas at the same centrality it is smaller in a smaller system.

For elliptic flow, $n = 2$, the ratio in Fig. 4(b) follows qualitatively the same trend as the ratio of values of ε_2 in Fig. 2(b): It is larger than 1 in the most central bins, which is due to the larger eccentricity fluctuations. It drops below 1 above 10% centrality, because of the smaller eccentricity in the reaction plane. We note that in central collisions the ratio of the v_2 coefficients is much smaller than the corresponding ratio for the spatial eccentricities of Fig. 2(b). This is an effect of viscous damping, which affects more strongly the smaller system, Xe+Xe. The situation is similar in peripheral collisions: The ratio of the initial eccentricities is close to unity above 50% centrality, while the v_2 ratio in hydro remains around 0.9, indicating larger viscous damping in the smaller system. Again, we show as a dashed line the ratio that one would obtain after hydrodynamic evolution of collisions of spherical ^{129}Xe nuclei: It is of the same order as the ratio of the v_3 coefficients (triangles) in very central collisions, and matches the v_2 ratio with deformed nuclei (circles) around 15% centrality.

Moving on to triangular flow, $n = 3$, the ratio in Fig. 4(b) is larger than 1 up to 40% centrality, in agreement with the ratio of the corresponding triangularities [Fig. 2(b)]. Above 40% centrality, however, viscous damping causes the v_3 ratio to drop below 1, even though the ratio of ε_3 does not.

Finally, the situation for v_4 is intermediate, as v_4 is driven by both fluctuations in the most central bins (ratio larger than unity), and nonlinear coupling to v_2 in mid-central and peripheral collisions [84] (ratio below unity). The latter feature also explains why v_4 is not affected by nuclear deformation effects.

C. Flow fluctuations

Cumulants of the probability distribution of anisotropic flow [79] are measured to a great accuracy [85–87], and give detailed insight into the statistical properties of v_n [88]. The first three cumulants of v_n fluctuations, which we expect to be experimentally accessible after the Xe+Xe run at the LHC, are defined by

$$v_n\{2\}^2 = \langle v_n^2 \rangle,$$
$$v_n\{4\}^4 = 2\langle v_n^2 \rangle^2 - \langle v_n^4 \rangle,$$
$$v_n\{6\}^6 = \tfrac{1}{4}\left(\langle v_n^6 \rangle - 9\langle v_n^2 \rangle \langle v_n^4 \rangle + 12\langle v_n^2 \rangle^3\right),$$

where angular brackets denote an average over events in a centrality bin.

By taking ratios of cumulants of different orders in the same harmonic n, one obtains direct information on the relative fluctuations of v_n [50]. The ratio $v_n\{4\}/v_n\{2\}$ is the simplest measure of relative fluctuations: it is equal to 1 if v_n is the same for all events, and smaller than 1 otherwise. Figure 5(a) displays our hydrodynamic results for this ratio, in the case $n = 2$, as a function of the collision centrality. Results are presented along with ALICE data on Pb+Pb collisions at $\sqrt{s_{\rm NN}} = 5.02$ TeV [78]. This ratio presents a distinctive feature: It first increases with centrality, and then changes trend. This is correctly predicted by hydrodynamics, and our results are in fair agreement with data. The remarkable point to note is that the ratio of cumulants of initial eccentricities, $\varepsilon_2\{4\}/\varepsilon_2\{2\}$, is somewhat larger than $v_2\{4\}/v_2\{2\}$, as a result of a nonlinear hydrodynamic response [89]. In particular, $\varepsilon_2\{4\}/\varepsilon_2\{2\}$ increases, and then saturates as a function of centrality percentile. This is a general feature of initial condition models [50]. Once the nonlinear hydrodynamic response is taken into account, however, one naturally recovers the nonmonotonic behavior of $v_2\{4\}/v_2\{2\}$. This shows that the success of the fluid-dynamical description of elliptic flow extends beyond the linear response to the initial eccentricity. Our prediction for Xe+Xe collisions is also shown in Fig. 5(a). At a given centrality, elliptic flow fluctuations are larger in Xe+Xe than in Pb+Pb, resulting in a smaller $v_2\{4\}/v_2\{2\}$ than for Pb+Pb collisions. Note that the difference between $\varepsilon_2\{4\}/\varepsilon_2\{2\}$ and $v_2\{4\}/v_2\{2\}$, due to nonlinear hydrodynamic response, is larger for Xe+Xe than for Pb+Pb.

Figure 5(b) presents the ratio $v_3\{4\}/v_3\{2\}$, which is significantly smaller than $v_2\{4\}/v_2\{2\}$, as triangular flow is solely due to fluctuations [30]. The ratio $v_3\{4\}/v_3\{2\}$ directly probes the non-Gaussianity of v_3 fluctuations [50,90], and non-Gaussian fluctuations of the initial triangularity ε_3 are expected as a consequence of finite-size corrections to the central limit theorem [29,91,92]. On this basis, one expects $\varepsilon_3\{4\}/\varepsilon_3\{2\}$ to scale with the number of participant nucleons N like $N^{-1/4}$. The results on this ratio provided by our initial condition models, displayed as full symbols in Fig. 5(b), follow the expected behavior: $\varepsilon_3\{4\}/\varepsilon_3\{2\}$ increases as a function of centrality percentile, and it is larger for Xe+Xe than for Pb+Pb. The ratio between Xe+Xe and Pb+Pb is close to the value 1.13 expected on the basis of $A^{-1/4}$ scaling. Note that the value of $v_3\{4\}/v_3\{2\}$ at the end of the hydrodynamic calculation is smaller than $\varepsilon_3\{4\}/\varepsilon_3\{2\}$, in particular above 30% centrality. This results in a flatter centrality dependence for $v_3\{4\}/v_3\{2\}$ than for $\varepsilon_3\{4\}/\varepsilon_3\{2\}$. These hydrodynamic results are consistent with experimental data [85,93,94] which so far do not show any clear centrality dependence of $v_3\{4\}/v_3\{2\}$ for Pb+Pb collisions. We do not seize any clear difference between the values of $v_3\{4\}/v_3\{2\}$ in Xe+Xe and in Pb+Pb collisions.

Finally, Fig. 5(c) displays the ratio $v_2\{6\}/v_2\{4\}$. This ratio is equal to 1 if the fluctuations of v_2 are Gaussian [52]. Hydrodynamics predicts its value to be slightly smaller than 1. This originates from the fact that the eccentricity in the reaction plane is bounded by unity, which skews the distribution of ε_2 [88]. The ratio $v_2\{6\}/v_2\{4\}$ is close to the corresponding ratios

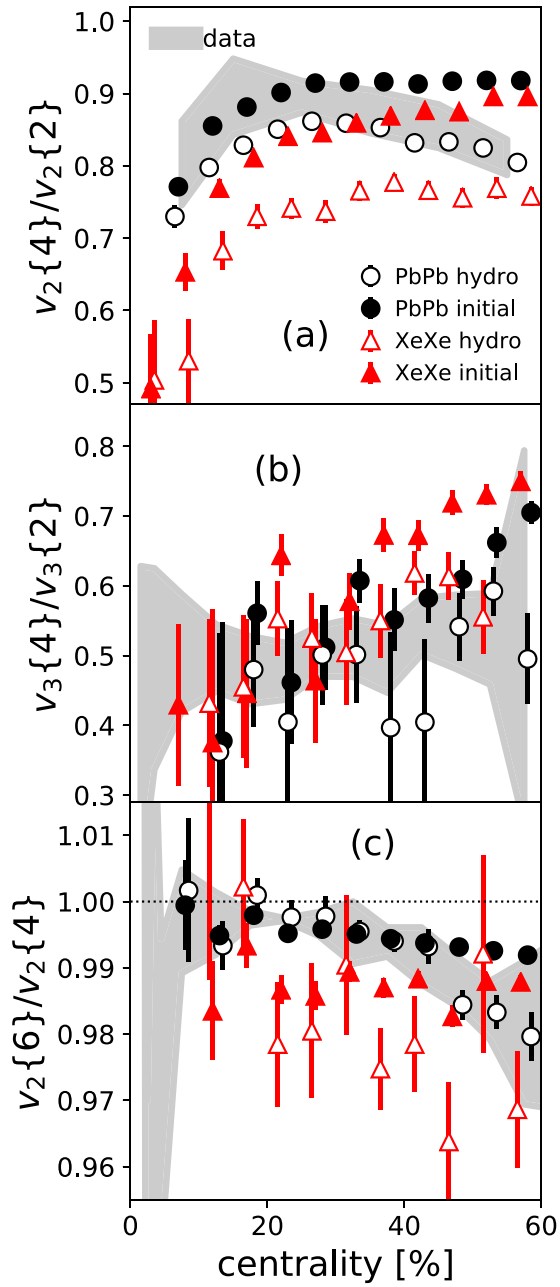

FIG. 5. Ratios of cumulants of anisotropic flow (open symbols) and corresponding ratios for initial eccentricity harmonics (full symbols), in Pb+Pb and Xe+Xe collisions from our hydrodynamic calculation, as a function of centrality percentile. From top to bottom: (a) $v_2\{4\}/v_2\{2\}$ and $\varepsilon_2\{4\}/\varepsilon_2\{2\}$. Data are from 5.02 TeV Pb+Pb collisions collected by the ALICE Collaboration [78]. (b) $v_3\{4\}/v_3\{2\}$ and $\varepsilon_3\{4\}/\varepsilon_3\{2\}$. Data are from 2.76 TeV Pb+Pb collisions collected by the ATLAS Collaboration [85]. (c) $v_2\{6\}/v_2\{4\}$ and $\varepsilon_2\{6\}/\varepsilon_2\{4\}$. Data are from 2.76 TeV Pb+Pb collisions collected by the ATLAS Collaboration [85].

for initial eccentricities $\varepsilon_2\{6\}/\varepsilon_2\{4\}$ for the most central bins and then becomes gradually smaller. Interestingly, experimental data for Pb+Pb collisions [85–87] are in perfect agreement with the full hydrodynamic calculation, and not with the ratio $\varepsilon_2\{6\}/\varepsilon_2\{4\}$ from the initial state. This underlines once more

that the success of hydrodynamics goes beyond linear response to ε_2. We predict a smaller value of $v_2\{6\}/v_2\{4\}$ in Xe+Xe collisions than in Pb+Pb collisions for all centralities.

Before concluding, we stress that we have explicitly checked the impact of the nuclear deformation on the presented ratios of cumulants. We find that the effect of switching off the deformation of the ^{129}Xe nuclei is smaller than the statistical error bars shown in Fig. 5, and, therefore, negligible in our calculation.

IV. CONCLUSIONS

We have presented predictions for upcoming data on Xe+Xe collisions at $\sqrt{s_{\rm NN}} = 5.44$ TeV at the LHC. Detailed comparisons with results from Pb+Pb collisions at $\sqrt{s_{\rm NN}} = 5.02$ TeV provide a unique opportunity to directly test fundamental scaling rules obeyed by hydrodynamic models. The mean transverse momentum is the same in Xe+Xe as in Pb+Pb collisions, the difference being at most 2% in mid-central collisions. Elliptic flow is larger by 25% in Xe+Xe (where 15% are due to the change in system size and 10% to the deformation of the ^{129}Xe nucleus) than in Pb+Pb in the 0–5% centrality window, but smaller by 10% above 30% centrality. Triangular flow is larger than in Pb+Pb collisions up to 30% centrality, and smaller above 40% centrality. The maximum value of the ratio $v_2\{4\}/v_2\{2\}$ is around 0.8 in Xe+Xe collisions, while it reaches 0.9 in Pb+Pb collisions. The relative difference between $v_2\{4\}$ and $v_2\{6\}$ is also significantly larger, typically by a factor 2, in Xe+Xe than in Pb+Pb collisions. The latter predictions on cumulant ratios probe the ability of hydrodynamics to model anisotropic flow in the nonlinear regime, beyond linear response to initial anisotropies.

ACKNOWLEDGMENTS

We thank the experimental physicists working at the CERN LHC for the useful input. We thank A. Toia for providing us with the ALICE data used in Fig. 1. J.N.H. acknowledges the Office of Advanced Research Computing (OARC) at Rutgers, The State University of New Jersey for providing access to the Amarel cluster, and associated research computing resources that have contributed to the results reported here. J.N.H also acknowledges the use of the Maxwell Cluster and the advanced support from the Center of Advanced Computing and Data Systems at the University of Houston. This work was funded under USP-COFECUB Project No. Uc Ph 160-16 (2015/13) and under FAPESP-CNRS Project No. 2015/50438-8. M.L. acknowledges support from FAPESP Projects No. 2016/24029-6 and No. 2017/05685-2, and INCT-FNA Proc. No. 464898/2014-5.

[1] U. Heinz and R. Snellings, Annu. Rev. Nucl. Part. Sci. **63**, 123 (2013).
[2] J. E. Bernhard, J. S. Moreland, S. A. Bass, J. Liu, and U. Heinz, Phys. Rev. C **94**, 024907 (2016).
[3] S. McDonald, C. Shen, F. Fillion-Gourdeau, S. Jeon, and C. Gale, Phys. Rev. C **95**, 064913 (2017).
[4] H. Niemi, K. J. Eskola, and R. Paatelainen, Phys. Rev. C **93**, 024907 (2016).
[5] H. Niemi, K. J. Eskola, R. Paatelainen, and K. Tuominen, Phys. Rev. C **93**, 014912 (2016).
[6] J. Y. Ollitrault, Phys. Rev. D **46**, 229 (1992).
[7] X. N. Wang, Nucl. Phys. A **750**, 98 (2005).
[8] B. Muller, J. Schukraft, and B. Wyslouch, Annu. Rev. Nucl. Part. Sci. **62**, 361 (2012).
[9] P. Bozek and W. Broniowski, Phys. Lett. B **718**, 1557 (2013).
[10] I. Kozlov, M. Luzum, G. Denicol, S. Jeon, and C. Gale, arXiv:1405.3976.
[11] R. D. Weller and P. Romatschke, Phys. Lett. B **774**, 351 (2017).
[12] V. Khachatryan *et al.* (CMS Collaboration), J. High Energy Phys. 09 (2010) 091.
[13] S. Chatrchyan *et al.* (CMS Collaboration), Phys. Lett. B **718**, 795 (2013).
[14] B. Abelev *et al.* (ALICE Collaboration), Phys. Lett. B **719**, 29 (2013).
[15] G. Aad *et al.* (ATLAS Collaboration), Phys. Lett. B **725**, 60 (2013).
[16] V. Khachatryan *et al.* (CMS Collaboration), Phys. Rev. Lett. **115**, 012301 (2015).
[17] V. Khachatryan *et al.* (CMS Collaboration), Phys. Lett. B **765**, 193 (2017).
[18] K. Dusling and R. Venugopalan, Phys. Rev. D **87**, 094034 (2013).
[19] E. Iancu and A. H. Rezaeian, Phys. Rev. D **95**, 094003 (2017).
[20] K. Dusling, M. Mace, and R. Venugopalan, Phys. Rev. D **97**, 016014 (2018).
[21] A. Esposito and M. Gyulassy, Phys. Lett. B **747**, 433 (2015).
[22] B. Blok, C. D. Jäkel, M. Strikman, and U. A. Wiedemann, J. High Energy Phys. 12 (2017) 074.
[23] S. Eremin and S. Voloshin, Phys. Rev. C **67**, 064905 (2003).
[24] P. Bożek, W. Broniowski and M. Rybczyński, Phys. Rev. C **94**, 014902 (2016).
[25] C. Loizides, Phys. Rev. C **94**, 024914 (2016).
[26] B. G. Zakharov, JETP Lett. **104**, 6 (2016) [Pisma Zh. Eksp. Teor. Fiz. **104**, 8 (2016)].
[27] B. Alver *et al.* (PHOBOS Collaboration), Phys. Rev. Lett. **98**, 242302 (2007).
[28] J. Takahashi, B. M. Tavares, W. L. Qian, R. Andrade, F. Grassi, Y. Hama, T. Kodama, and N. Xu, Phys. Rev. Lett. **103**, 242301 (2009).
[29] R. S. Bhalerao, M. Luzum, and J. Y. Ollitrault, Phys. Rev. C **84**, 054901 (2011).
[30] B. Alver and G. Roland, Phys. Rev. C **81**, 054905 (2010); **82**, 039903(E) (2010).
[31] F. Cooper and G. Frye, Phys. Rev. D **10**, 186 (1974).
[32] N. Borghini and J. Y. Ollitrault, Phys. Lett. B **642**, 227 (2006).
[33] R. Baier, P. Romatschke, D. T. Son, A. O. Starinets, and M. A. Stephanov, J. High Energy Phys. 04 (2008) 100.
[34] P. Romatschke and U. Romatschke, Phys. Rev. Lett. **99**, 172301 (2007).
[35] P. Möller, A. J. Sierk, T. Ichikawa, and H. Sagawa, At. Data Nucl. Data Tables **109-110**, 1 (2016).
[36] M. Luzum and P. Romatschke, Phys. Rev. C **78**, 034915 (2008); **79**, 039903(E) (2009).

[37] C. Shen and U. Heinz, Nucl. Phys. News **25**, 6 (2015).
[38] E. Retinskaya, M. Luzum, and J. Y. Ollitrault, Phys. Rev. C **89**, 014902 (2014).
[39] J. D. Bjorken, Phys. Rev. D **27**, 140 (1983).
[40] J. S. Moreland, J. E. Bernhard, and S. A. Bass, Phys. Rev. C **92**, 011901 (2015).
[41] C. Loizides, J. Nagle, and P. Steinberg, SoftwareX **1-2**, 13 (2015).
[42] (ALICE Collaboration), ALICE-PUBLIC-2015-008, https://cds.cern.ch/record/2118084?ln=en.
[43] G. Aad *et al.* (ATLAS Collaboration), Phys. Lett. B **707**, 330 (2012).
[44] S. Chatrchyan *et al.* (CMS Collaboration), J. High Energy Phys. 08 (2011) 141.
[45] B. Abelev *et al.* (ALICE Collaboration), Phys. Rev. C **88**, 044909 (2013).
[46] S. J. Das, G. Giacalone, P. A. Monard, and J. Y. Ollitrault, Phys. Rev. C **97**, 014905 (2018).
[47] (ATLAS Collaboration), ATLAS-CONF-2017-066, https://cds.cern.ch/record/2285570.
[48] B. Alver *et al.* (PHOBOS Collaboration), Phys. Rev. C **83**, 024913 (2011).
[49] D. Teaney and L. Yan, Phys. Rev. C **83**, 064904 (2011).
[50] G. Giacalone, J. Noronha-Hostler, and J. Y. Ollitrault, Phys. Rev. C **95**, 054910 (2017).
[51] Z. Qiu and U. W. Heinz, Phys. Rev. C **84**, 024911 (2011).
[52] S. A. Voloshin, A. M. Poskanzer, A. Tang, and G. Wang, Phys. Lett. B **659**, 537 (2008).
[53] L. Adamczyk *et al.* (STAR Collaboration), Phys. Rev. Lett. **115**, 222301 (2015).
[54] J. Noronha-Hostler, G. S. Denicol, J. Noronha, R. P. G. Andrade, and F. Grassi, Phys. Rev. C **88**, 044916 (2013).
[55] J. Noronha-Hostler, J. Noronha, and F. Grassi, Phys. Rev. C **90**, 034907 (2014).
[56] J. Noronha-Hostler, J. Noronha, and M. Gyulassy, Phys. Rev. C **93**, 024909 (2016).
[57] S. Borsanyi, Z. Fodor, C. Hoelbling, S. D. Katz, S. Krieg, and K. K. Szabo, Phys. Lett. B **730**, 99 (2014).
[58] P. F. Kolb, P. Huovinen, U. W. Heinz, and H. Heiselberg, Phys. Lett. B **500**, 232 (2001).
[59] J. Vredevoogd and S. Pratt, Phys. Rev. C **79**, 044915 (2009).
[60] W. van der Schee, P. Romatschke, and S. Pratt, Phys. Rev. Lett. **111**, 222302 (2013).
[61] J. Liu, C. Shen, and U. Heinz, Phys. Rev. C **91**, 064906 (2015); **92**, 049904(E) (2015).
[62] L. Keegan, A. Kurkela, A. Mazeliauskas, and D. Teaney, J. High Energy Phys. 08 (2016) 171.
[63] P. Alba, V. M. Sarti, J. Noronha, J. Noronha-Hostler, P. Parotto, I. P. Vazquez, and C. Ratti, arXiv:1711.05207.
[64] J. Noronha-Hostler, J. Noronha, and C. Greiner, Phys. Rev. Lett. **103**, 172302 (2009).
[65] A. Monnai and T. Hirano, Phys. Rev. C **80**, 054906 (2009).
[66] P. Bozek, Phys. Rev. C **81**, 034909 (2010).
[67] D. Teaney, Phys. Rev. C **68**, 034913 (2003).
[68] C. Patrignani *et al.* (Particle Data Group), Chin. Phys. C **40**, 100001 (2016).
[69] P. Alba *et al.*, Phys. Rev. D **96**, 034517 (2017).
[70] H. Song, S. A. Bass, U. Heinz, T. Hirano, and C. Shen, Phys. Rev. C **83**, 054910 (2011); **86**, 059903(E) (2012).
[71] P. F. Kolb and R. Rapp, Phys. Rev. C **67**, 044903 (2003).
[72] B. Abelev *et al.* (ALICE Collaboration), Phys. Rev. C **88**, 044910 (2013).
[73] J. Noronha-Hostler, M. Luzum, and J. Y. Ollitrault, Phys. Rev. C **93**, 034912 (2016).
[74] S. Ryu, J.-F. Paquet, C. Shen, G. S. Denicol, B. Schenke, S. Jeon, and C. Gale, Phys. Rev. Lett. **115**, 132301 (2015).
[75] A. Monnai and J. Y. Ollitrault, Phys. Rev. C **96**, 044902 (2017).
[76] J. Adam *et al.* (ALICE Collaboration), Phys. Rev. Lett. **116**, 222302 (2016).
[77] M. Luzum, J. Phys. G **38**, 124026 (2011).
[78] J. Adam *et al.* (ALICE Collaboration), Phys. Rev. Lett. **116**, 132302 (2016).
[79] N. Borghini, P. M. Dinh, and J. Y. Ollitrault, Phys. Rev. C **64**, 054901 (2001).
[80] B. H. Alver, C. Gombeaud, M. Luzum, and J. Y. Ollitrault, Phys. Rev. C **82**, 034913 (2010).
[81] M. Luzum and J. Y. Ollitrault, Nucl. Phys. A **904-905**, 377c (2013).
[82] H. Niemi, G. S. Denicol, H. Holopainen, and P. Huovinen, Phys. Rev. C **87**, 054901 (2013).
[83] C. Gombeaud and J. Y. Ollitrault, Phys. Rev. C **77**, 054904 (2008).
[84] F. G. Gardim, F. Grassi, M. Luzum, and J. Y. Ollitrault, Phys. Rev. C **85**, 024908 (2012).
[85] G. Aad *et al.* (ATLAS Collaboration), Eur. Phys. J. C **74**, 3157 (2014).
[86] B. B. Abelev *et al.* (ALICE Collaboration), Phys. Rev. C **90**, 054901 (2014).
[87] A. M. Sirunyan *et al.* (CMS Collaboration), arXiv:1711.05594.
[88] G. Giacalone, L. Yan, J. Noronha-Hostler, and J. Y. Ollitrault, Phys. Rev. C **95**, 014913 (2017).
[89] J. Noronha-Hostler, L. Yan, F. G. Gardim, and J. Y. Ollitrault, Phys. Rev. C **93**, 014909 (2016).
[90] N. Abbasi, D. Allahbakhshi, A. Davody, and S. F. Taghavi, arXiv:1704.06295.
[91] L. Yan and J. Y. Ollitrault, Phys. Rev. Lett. **112**, 082301 (2014).
[92] H. Grönqvist, J. P. Blaizot, and J. Y. Ollitrault, Phys. Rev. C **94**, 034905 (2016).
[93] K. Aamodt *et al.* (ALICE Collaboration), Phys. Rev. Lett. **107**, 032301 (2011).
[94] S. Chatrchyan *et al.* (CMS Collaboration), Phys. Rev. C **89**, 044906 (2014).